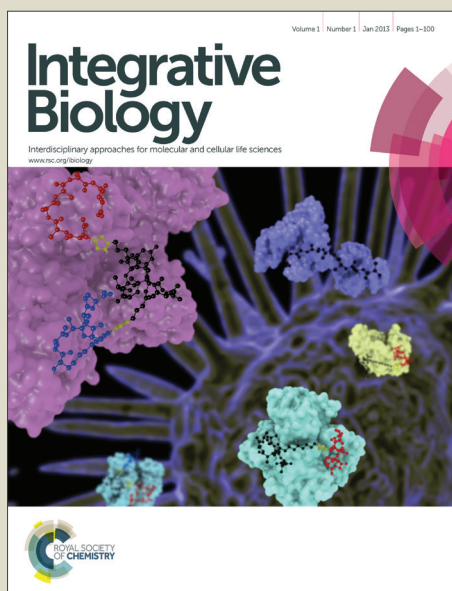


Integrative Biology

Accepted Manuscript



This is an *Accepted Manuscript*, which has been through the Royal Society of Chemistry peer review process and has been accepted for publication.

Accepted Manuscripts are published online shortly after acceptance, before technical editing, formatting and proof reading. Using this free service, authors can make their results available to the community, in citable form, before we publish the edited article. We will replace this *Accepted Manuscript* with the edited and formatted *Advance Article* as soon as it is available.

You can find more information about *Accepted Manuscripts* in the [Information for Authors](#).

Please note that technical editing may introduce minor changes to the text and/or graphics, which may alter content. The journal's standard [Terms & Conditions](#) and the [Ethical guidelines](#) still apply. In no event shall the Royal Society of Chemistry be held responsible for any errors or omissions in this *Accepted Manuscript* or any consequences arising from the use of any information it contains.

INSIGHT BOX

The heparan sulfate component of the endothelial cell (EC) glycocalyx (GCX) enables transduction of blood flow forces into biological functions that are important for vascular health. Little is known about the involvement of the specific heparan sulfate core proteins—membrane anchored glypican and the trans-membrane anchored syndecans—in mechanotransmission, and their modes of operation. From an engineering perspective and by applying cell and molecular biology approaches, we studied flow-conditioned wildtype, glypican-1 knockdown, and syndecan-1 knockdown EC behavior. We deciphered the roles of these proteins in diverse flow-induced biomolecular and biomechanical functions. We generated new knowledge that is essential for the development of methods to re-constitute or reinforce the GCX in order to restore critical EC functions and treat vascular disease.

**Shear-induced Endothelial NOS Activation and Remodeling
via Heparan Sulfate, Glypican-1, and Syndecan-1**

Eno E Ebong, Ph.D.^{a,b,*}, Sandra V Lopez-Quintero, PhD.^a, Victor Rizzo, Ph.D.^c, David C Spray,
Ph.D.^a, and John M Tarbell, Ph.D.^b

^a Department of Neuroscience, Albert Einstein College of Medicine,
1300 Morris Park Ave, K-840, Bronx, NY 10461

^b Department of Biomedical Engineering, City College of New York,
140th Street and Convent Avenue, T-404B, New York, NY 10031

^c Cardiovascular Research Center, Temple University School of Medicine,
3500 N. Broad Street, MERB 1080, Philadelphia, PA 19140

January 8, 2014

*Address for correspondence and current affiliation:

Eno E. Ebong, Ph.D.

Department of Chemical Engineering

Northeastern University

360 Huntington Avenue, 313 Snell

Boston, MA 02115

Tel: (617) 373-8744

Fax: (617) 373-2209

e-mail: e.ebong@neu.edu

Short Title: HS/GPC1/SDC1 Regulation of eNOS and EC Remodeling

TABLE OF CONTENTS ENTRY

This work uncovers new mechanisms of endothelial cell glycocalyx mediated conversion of fluid forces into diverse biomolecular and biomechanical responses, such as caveola associated signaling and cytoskeleton reorganization.

ABSTRACT

Mammalian epithelial cells are coated with a multifunctional surface glycocalyx (GCX). On vascular endothelial cells (EC), intact GCX is atheroprotective. It is degraded in many vascular diseases. GCX heparan sulfate (HS) is essential for healthy flow-induced EC nitric oxide (NO) release, elongation, and alignment. The HS core protein mechanisms involved in these processes are unknown. We hypothesized that the glypican-1 (GPC1) HS core protein mediates flow-induced EC NO synthase (eNOS) activation because GPC1 is anchored to caveolae where eNOS resides. We also hypothesized that the HS core protein syndecan-1 (SDC1) mediates flow-induced EC elongation and alignment because SDC1 is linked to the cytoskeleton which impacts cell shape. We tested our hypotheses by exposing EC monolayers treated with HS degrading heparinase III (HepIII), and monolayers with RNA-silenced GPC1, or SDC1, to 3 to 24 hours of physiological shear stress. Shear-conditioned EC with intact GCX exhibited characteristic eNOS activation in short-term flow conditions. After long-term exposure, EC with intact GCX were elongated and aligned in the direction of flow. HS removal and GPC1 inhibition, not SDC1 reduction, blocked shear-induced eNOS activation. EC remodeling in response to flow was attenuated by HS degradation and in the absence of SDC1, but preserved with GPC1 knockdown. These findings clearly demonstrate that HS is involved in both centralized and decentralized GCX-mediated mechanotransduction mechanisms, with GPC1 acting as a centralized mechanotransmission agent and SDC1 functioning in decentralized mechanotransmission. This foundational work demonstrates how EC can transform fluid shear forces into diverse biomolecular and biomechanical responses.

Key Words:

Endothelial Cell, Mechanotransduction, Heparan sulfate, Syndecan-1, Glypican-1

INTRODUCTION

The extracellular surface glycocalyx (GCX) coat on epithelial cells and many other cell types facilitates cell-cell recognition, communication and signaling, and cell-cell and cell-substrate adhesion¹. In the vasculature, an intact GCX coat on blood vessel wall endothelial cells (EC) enables EC functions that are important for vascular health²⁻⁵. A degraded GCX promotes EC dysfunction that leads to atherosclerosis^{6, 7} - the underlying cause of most heart attacks, strokes, aneurysms, and peripheral vascular disorders^{8, 9}. In the present study, we investigate mechanisms by which the GCX initiates EC mechanotransduction, recognizing that many other cell types including vascular smooth muscle cells¹⁰⁻¹⁴ and cancer cells¹⁵ transduce fluid flow shear stresses into important biological responses.

The single layer of EC that line the inner surfaces of blood vessels is placed in a unique position at the interface between circulating blood and underlying tissue. As a result, the endothelium senses changes in the blood flow environment through fluid shear stress at the EC surface and pressure-induced stretch, and performs mechano-remodeling and mechano-signaling functions that maintain physiological vascular function and defend the integrity of the vascular wall. Perhaps the two most widely recognized flow-induced EC responses are the dramatic elongation and alignment of EC in the axial direction of undisturbed flow, and nitric oxide (NO) dependent vasoactivity, among many others^{16, 17}. In disturbed flow conditions where shear stress has a low mean and highly oscillatory character, EC are not elongated, taking on a cobblestone-shaped morphology, and NO dependent vasoactivity is impaired¹⁷. EC conversion of fluid mechanical forces into biological responses—mechanotransduction—can be centralized or decentralized. In the centralized case, mechanotransduction occurs at a primary site of the luminal cell surface where shear is sensed¹⁸. In the decentralized case, force is transmitted to remote sites via the cytoskeleton¹⁸ where mechanotransduction occurs.

Many centralized and decentralized EC mechanotransduction events are regulated by the surface glycocalyx (GCX)²⁻⁵ which acts as an initial mechanotransmitter. The GCX is a hydrated structure containing a wide variety of blood-borne and membrane-bound macromolecules¹⁹, including

glycosaminoglycans (GAGs) bound to core proteins (proteoglycans). Heparan sulfate (HS) is the most prominent endothelial GCX GAG and makes up over 50% of the total GAG content ²⁰. The proteoglycan core proteins that covalently bind HS are the transmembrane syndecans (SDC)—SDC1, 2, and 4—and the membrane bound glypican—GPC1—that is linked to lipid rafts and caveolae ²¹. Among the syndecans, SDC1 is mainly apical, and SDC2 and SDC4 are primarily basal. The syndecans have extracellular HS binding sites near their N-terminus, remote from their transmembrane attachment point ^{22, 23}. SDC1 also contains extracellular chondroitin sulfate (CS) linkage sites closer to the membrane ²⁴. On the cytoplasmic side of the plasma membrane, the syndecan tails associate with the cytoskeleton ²⁵ and assist in its organization, through molecules including tubulin and dynamin ²⁶. Glypican, on the other hand, is entirely extracellular, lies close to the plasma membrane, and covalently binds HS and no other GAG ²⁷. GPC1 is bound to the plasma membrane through a C-terminal glycosylphosphatidylinositol (GPI) anchor ²⁷. GPC1 resides in the cholesterol- and sphingolipid-rich membrane rafts, particularly caveolae, which are involved in cell signaling ²⁷⁻²⁹. Within caveolae, GPC1 has the potential to interact with numerous flow-regulated signaling molecules including endothelial-type nitric oxide synthase (eNOS) ³⁰. Heparan sulfate GAG together with its syndecan and glypican proteoglycans, as well as other GCX components, are continuously shed and synthesized by EC in order to adapt to local environmental changes ³¹⁻³⁶ such as alterations in blood flow.

The GCX layer senses fluid shear stress through its GAG components and transmits mechanical force through the solid core proteins to cellular sites where mechanotransduction takes place ⁴. We have shown that degradation of HS, using heparinase III (HepIII), inhibits mechanotransduction events that occur at the cell membrane, in the cytoskeleton, and at the intercellular junctions. For example, shear induced NO production by cultured bovine aortic endothelial cells (BAEC) over 3 hrs was completely blocked when cells were pretreated with 15 mU/mL of HepIII ². ³ In the same cell type, shear-induced elevation in NO production led to increased endothelial layer hydraulic conductivity, but the response was blocked when HS was compromised by HepIII treatment ³⁷. Rat fat pad endothelial cells (RFPEC) exposed for 5 hours to 11 dyne/cm² fluid shear stress exhibit

F-actin stress fiber formation, vinculin migration to cell borders, and transient tight junction (ZO-1) and gap junction (Cx43) disruption when HS is intact ⁴. These responses were inhibited when HS was enzymatically degraded ⁴. In other studies, BAEC treatment with HepIII blocked 24-hour shear-induced EC elongation and alignment in the direction of flow as well as flow-induced suppression of EC proliferation ⁵. These studies confirm that endothelial GCX HS is essential for flow-induced cell signaling and related remodeling. However, the HS core proteins involved in these mechanotransduction events are unknown.

We hypothesize that GPC1 is the heparan sulfate proteoglycan (HSPG) that mediates flow-induced NO signaling via eNOS activation that occurs in plasma membrane caveolae where GPC1 is anchored. To our knowledge, GPC1 has no direct association with the cytoskeleton, which suggests that GPC1 plays no role in flow-induced EC remodeling. We further hypothesized that SDC1 is the core protein involved in flow-induced EC remodeling through its association with the cytoskeleton by which it can transmit signals to basal adhesion plaques, intercellular junctions, and other cellular sites. We believe that SDC1 is more likely than SDC2 and SDC4 to participate in flow-induced EC remodeling because of its location on the apical endothelial surface in direct contact with fluid shear stress. Although syndecans interact with signaling molecules which are involved in eNOS activation, such as protein kinase C- α ³⁸, the fact that they lie outside of the caveolae where the majority of membrane associated eNOS is stored ³⁹ suggests that SDC1 plays a secondary role in flow-induced EC signaling via eNOS.

To test our hypotheses, BAECs with intact GCX, HepIII degraded HS, RNA-silenced GPC1, or RNA-silenced SDC1 were exposed to 12 to 15 dyn/cm² steady shear stress for 3 to 24 hours. Total and activated (ser1177 phosphorylated) eNOS protein were measured, cell morphology was evaluated, and cytoskeletal organization was assessed. The results confirm our hypotheses and demonstrate the selectivity of GCX core proteins in mediating the two most characteristic mechanotransduction events associated with EC function.

RESULTS

Enzymatic Removal of HS: Recently, we demonstrated that cultured BAEC contain abundant HS embedded within a substantial glycocalyx⁴⁰. Using immunofluorescence, we verified the presence of HS on untreated confluent BAEC monolayers and confirmed the efficiency of HepIII induced HS cleavage. Approximately 67% of the HS surface was fluorescently labeled with HS antibodies under normal conditions, whereas treatment of the BAEC monolayer with 15 mU/mL of HepIII for 2 hours reduced coverage to 46% (Figure 1).

Knockdown of GPC1 and SDC1: Densitometric analysis of Western blots demonstrated that transfecting BAEC with glypican-1 or syndecan-1 shRNA successfully knocked down expression of the targeted glycocalyx core proteins. Transfection of glypican-1 shRNA resulted in a $72.5 \pm 0.05\%$ reduction of glypican-1 (Figure 2C). However, glypican-1 shRNA also reduced non-target syndecan-1 protein expression by $36.7 \pm 0.03\%$ (Figure 2C). Syndecan-1 shRNA resulted in $62.0 \pm 0.09\%$ reduction of syndecan-1 in BAEC (Figure 2D). Syndecan-1 shRNA had no effect on non-target glypican-1 expression (Figure 2D). For control purposes, we initially confirmed that BAEC treatment with the transfection media, reagent, and vector—OptiMEM, Optifect, and scrambled shRNA or GFP-expressing vector—induced no toxicity and no change in SDC1 or GPC1 expression levels (Figure 2B). We visualized the GFP-expressing vector transfected in live BAEC to see in real-time how effectively the RNA interfering shRNA was delivered into and then stabilized in BAEC cultures. The efficiency of the stable shRNA transfection, as indicated by the percentage of BAEC expressing the GFP control shRNA, was 80% to 90% (Figure 2A). HS immunofluorescence results from additional control experiments confirmed the loss of HS coincident with primary reduction of GPC1 core protein expression and secondary reduction of SDC1 core protein expression using the GPC1 shRNA (Supplemental Figure 1). These control experiments were not performed on SDC1 shRNA treated BAEC, due to the untimely discontinuation of the commercially available HS antibody that was used for this study.

HS and GPC1 Knockdown, but not SDC1, Inhibit Flow-induced eNOS Activation: Shown in figure 3 are representative Western blots (Figs 3A, 3C, and 3E) and their densitometric quantification (Figs 3B, 3D, and 3F) from BAEC exposed to (i) no-flow control and (ii) 3-hours shear stress. Figures 3A and 3B correspond to HS-degraded monolayers, figures 3C and 3D to GPC1-silenced monolayers and figures 3E and 3F to SDC1-silenced monolayers. In addition to probing for ser1177 phosphorylated eNOS (p-eNOS), we probed for total eNOS and β -actin. Total eNOS was insensitive to shear stress and other treatments, as was β -actin, the internal loading control. The densitometric analysis shows that, the expression of p-eNOS (normalized by total eNOS) in BAEC exposed to shear stress was significantly up regulated in the 3 sets of experiments by 2.1 ± 0.5 to 2.9 ± 0.9 fold relative to unsheared controls.

Up regulation of p-eNOS by shear stress was completely abolished by HepIII treatment (Figs 3A and 3B). Notably, treating unsheared control BAEC with HepIII had a negligible effect on p-eNOS expression compared to untreated/unsheared BAEC (Figs 3A and 3B), indicating that HS does not participate in eNOS activation in static conditions but only in the presence of flow. The shear stress- and HS-regulated changes in eNOS phosphorylation are consistent with previously reported alteration in shear-induced NO production in BAEC that was completely blocked by treatment with Hep III at the same concentration we have used [3, 4].

Knockdown of the HS-binding core protein GPC1, along with off-target low level knockdown of SDC1, completely blocked shear-induced activation of p-eNOS (Fig 3 C,D). In static controls, the p-eNOS levels of untreated BAECs and GPC1-silenced BAEC were similar. Thus, like HS, GPC1 does not participate in eNOS activation in static conditions but only in the presence of flow. The question remains whether or not SDC1 knockdown by GPC1 shRNA (Fig 2) contributes to the inhibition of shear-induced p-eNOS.

To address this point, when BAEC were transfected with SDC1 shRNA, which exclusively targets SDC1 and not GPC1 (Fig 2), flow-induced p-eNOS expression was not inhibited (Figs 3E and

3F). There was a small but significant increase in p-eNOS expression of unsheared SDC1 knockdowns compared to untreated unsheared BAEC conditions, but shear-induced p-eNOS was still up-regulated significantly relative to the SDC1 knockdown static controls.

HS and SDC1, but not GPC1, Regulate Flow-induced Endothelial Cell Remodeling: Figure 4 shows representative phase contrast images of BAEC after 24-hour exposure to static control conditions or 15 dynes/cm² average shear stress, along with quantification of cell elongation and alignment. The results indicate the significant role of HS, and the insignificant role of the HS core protein GPC1, in EC remodeling. Control endothelial cells (untreated and unsheared) exhibited a near cobblestone morphology (Fig 4A) with aspect ratios of ranging from 1.75 to 1.85, depending on the EC batch. Fold changes in aspect ratio are presented in figure 4E, so the aspect ratio of the control EC shown in figure 4A has a value of 1 (normalized). These cells show no particular orientation, as indicated by the angles of their major axis with respect to the flow direction that were distributed randomly at all angles from 0° to ± 90° (Figures 4F to 4H, grey bars). As expected, untreated ECs exposed to flow were elongated and aligned in the direction of flow after 24 hours, with a fold increase in aspect ratio to 2.1 ± 0.05 (Figures 4B and 4E). The major axes of $55 \pm 5\%$ of the flow-conditioned cells (compared to ~12% of the static conditioned cells) were oriented between 0° and ± 10° with respect to the direction of flow (Figure 4F, black bars).

HS degradation by HepIII treatment statistically significantly reduced shear- induced elongation (Fig 4 C, E) and completely abolished alignment (Fig 4 C, G). The fold increase was only 1.3 ± 0.3 in HepIII-treated sheared BAEC, compared to 2.1 ± 0.05 in untreated BAEC (Figs 4C and 4E). In comparison to untreated sheared BAEC, HepIII-treated cells were not aligned in the direction of flow with only $18 \pm 3\%$ of cells oriented between 0° and ± 10° relative to the flow direction (Fig 4G, black bars). Knockdown of glypican-1 preserved most EC remodeling under flow. Shear-conditioned GPC1-silenced BAEC were elongated to a 2.0 ± 0.3 fold increased aspect ratio compared to 2.1 ± 0.05 in untreated BAEC (Figures 4D and 4E) and $38 \pm 4\%$ of cells were oriented between 0° and ± 10° relative to flow (Figure 4H, black bars).

We attempted to perform similar 24-hour cell remodeling experiments with SDC1 shRNA-treated BAEC. We found, however, that BAEC monolayers with reduced SDC1 expression were unable to maintain their integrity under long term shear. Thirty to 40 percent of cells were lost from the monolayer after flow conditioning (Supplemental Figure 2). In lieu of 24-hour studies of SDC1 knockdown remodeling, 6-hour experiments were undertaken. In these experiments, we performed phase contrast microscopy together with cell aspect ratio and orientation angle analysis. In addition, confocal microscope immunofluorescence images of stained f-actin fibers were qualitatively assessed. The results of these experiments are summarized in figure 5. We observed and confirmed that control EC exhibit cobblestone shape morphology and show no preferential alignment in any angle from 0° to $\pm 90^\circ$ angle (Figure 5A, grey e in Figure 5E, and grey columns in Figure 5F). Control BAEC f-actin fibers were organized randomly within the cell body (Figures 5A). After 6 hours of flow exposure, untreated ECs showed the beginnings of elongation with a 1.14 ± 0.02 fold increase in aspect ratio (Fig 5D). 6-hr flow-conditioned EC showed the start of inclination towards the direction of flow, with the major axes of 17 ± 3 % of the flow-conditioned cells (compared to $\sim 8.5\%$ of the static conditioned cells) oriented between 0° and $\pm 10^\circ$ with respect to the direction of flow (Figure 5B and black columns in 5E). Untreated BAEC that were shear conditioned for 6 hours displayed f-actin fibers that were well oriented in the direction of the cellular long axis (Figure 5B). Knockdown of SDC1 interrupted EC remodeling during 6 hours of flow. Shear-conditioned and SDC1-silenced BAEC showed no change in aspect ratio (Fig 5D) and no preferred orientation relative to static controls (Fig 5F). Angles were distributed nearly equally in all possible directions (Figure 5C, 5D, and black columns in 5F). The f-actin fibers in sheared knockdown cells appeared just as disorganized as those of untreated and unsheared controls (Figure 5C).

DISCUSSION

The endothelial GCX plays an important role in sensing, transmitting and transducing EC surface fluid mechanical forces into biological responses at the cell membrane, cytoskeleton, basal adhesion plaques, and intercellular junctions. The importance of HS as a mechanosensor and mechanotransmitter in mediating flow-induced NO release and cell remodeling has been well demonstrated *in vitro* and *in vivo* ^{2, 3, 5, 41-47}.

In the present study, we determined the core proteins that mediate the NO and remodeling responses by manipulating (i) the HS GPC1 core protein that is bound to caveolae ²⁷⁻²⁹ where it may interact with eNOS and (ii) the transmembrane HS SDC1 core protein ^{22, 23} that has a linkage with the cytoskeleton ²⁵ which determines cell shape.

Using BAEC monolayers whose mechanotransduction characteristics are well known, we degraded HS with HepIII enzyme; knocked down GPC1 expression with GPC1 shRNA transfection; and knocked down SDC1 expression by SDC1 shRNA transfection. Our measured 67% HS fluorescence intensity on untreated BAEC monolayers (Fig 1) corroborates HS coverage on EC as measured by Megens et al ⁴⁸ and Robinson and Gospodarowicz ⁴⁹. The 15 mU/mL HepIII concentration that we used and the 46% HepIII-induced decrease in HS fluorescence (Fig 1) are in agreement with our previously reported mechanotransduction studies ^{4, 5, 48, 49}. Therefore, we are confident that we degraded enough HS on our cultured BAEC to effectively block flow-induced endothelial NOS activation and remodeling. We previously reported that less than 5% of non-targeted GCX components are removed by this concentration of HepIII ⁵⁰. Thus we know that the enzyme allowed us to study the effects of HS selectively.

Since HepIII treatment leaves the GPC1 and SDC1 core proteins intact, we selectively silenced GPC1 or SDC1 by RNA interference in order to determine if there was a resultant loss of mechanotransmission similar to what we and others have observed in response to HS degradation. In silencing GPC1 by 73%, we also reduced SDC1 by 37% (Fig 2C). The GPC1 shRNA sequence does not share complementarity with the SDC1 transcript, and therefore, simultaneous knockdown of GPC1

and SDC1 is not an off-target effect of the shRNA itself. An explanation for the double hit effect of the GPC1 shRNA may simply be that glypican-1 removal disrupts HS binding to syndecan-1 and subsequently interferes with HS dependent transmembrane anchoring of syndecan-1. Fortunately, direct silencing of SDC1 did not noticeably impact GPC1 (Fig 2D), enabling us to separate GPC1-dependent mechanotransmission from SDC1-dependent mechanotransmission.

We observed HS-dependent, flow-induced eNOS phosphorylation (Fig 3 A,B) that is consistent with previously reported alterations in NO production, also dependent on flow and the presence or absence of HS [3, 4]. Substantial knockdown of GPC1 along with a lesser reduction in SDC1 completely blocked shear-induced eNOS phosphorylation (Fig 3C and 3D), similar to that associated with HS degradation. This complete suppression of flow-induced eNOS phosphorylation is due solely to the loss of GPC1, because flow-induced p-eNOS remains significantly elevated following exclusive SDC1 knockdown (Fig 3 E,F). These results confirm that GPC1 is the major HSPG core protein regulator of flow-induced eNOS phosphorylation. We have supplementary data that further supports this conclusion. Figure S3 shows data from membrane fractionation experiments that clearly indicate the co-localization of GPC1 and caveolin-1 in the membrane raft fraction. More specifically, GPC1 is present in caveolae membranes where its expression increases in response to flow.

In agreement with previous reports ^{4, 5}, our results demonstrate that HS is required for flow-induced changes in EC shape to occur (Fig 4). In contrast, knockdown of GPC1 has little effect on flow-induced changes in cell morphology (Fig 4). EC elongation after 24-hour flow exposure is completely preserved with 73% reduced GPC1 expression (Fig 4). EC alignment is also largely preserved (Fig 4). Specifically, flow induced alignment of $55 \pm 5\%$ of untreated cells, while a still significant $38 \pm 4\%$ of GPC1-silenced cells became aligned in the direction of flow. The percent alignment difference between the two conditions was not found to be statistically significant. Partial (37%) reduction of SDC1 as a side effect of GPC1 shRNA transfection may have been the reason why GPC1-silenced EC alignment in the direction of 24-hour flow was somewhat reduced compared to the untreated EC (Fig 4).

The effect of SDC1 knockdown on flow-induced EC remodeling was more difficult to assess. BAEC monolayers with substantially (67%) reduced SDC1 expression could not maintain their integrity under 24-hour shear (supplemental Fig 2). We suspect that when SDC1 is substantially reduced it is not available to function as a co-factor for proteins that are responsible for stabilizing cell-cell or cell-substrate adhesion. Integrins are likely co-factors for SDC1. Previous studies of SDC1-deficient cells and mice indicate that SDC1 regulates cell adhesion and spreading via integrins^{51, 52}. In our study, it is likely that the reduction of SDC1 disrupts the integrin attachments. In the absence of robust integrin attachments, it is difficult to study the role of SDC1 in 24-hr flow-induced EC elongation and alignment.

Therefore we decided to perform shorter term 6-hour shear experiments in which the EC cytoskeleton becomes noticeably reorganized and the EC bodies begin to incline in the direction of flow. The knockdown of SDC1 inhibited 6-hr flow-induced cytoskeleton reorganization, elongation and inclination towards the flow direction (Fig 5), suggesting that SDC1 is in fact essential for the cytoskeleton to sense extracellular flow and for EC remodeling to occur. Due to the fact that we observed SDC1 shRNA treatment to disrupt cell adhesion and integrity in the long-term flow experiment, one might interpret integrin inactivation to be partly responsible for reduced cytoskeleton reorganization following SDC1 shRNA transfection in EC in 6 h experiments. We can not rule out this possibility at the present time although we did not observe any changes in cell morphology that would be indicative of altered cell-substrate adhesion in the 6h experiments.

In summary, we have shown that GPC1 and SDC1 selectively participate in two distinct and well-characterized flow-regulated EC functions. GPC1 mediates shear-induced eNOS activation but not EC remodeling in response to flow. SDC1 is involved flow-induced EC elongation, alignment, and cytoskeleton reorganization and plays no role in flow-induced eNOS activation.

MATERIALS AND METHODS

Cell Culture: BAEC were obtained from Lonza Walkersville, Inc. (Walkersville, MD). Cells were grown in tissue culture dishes according to Lonza instructions in EGM-MW growth medium supplemented with 5% fetal bovine serum (FBS), 0.04% hydrocortisone, 0.4% human fibroblast growth factor, 0.1% vascular endothelial growth factor, 0.1% R3-insulin-like growth factor-1, 0.1% ascorbic acid, 0.1% human recombinant epidermal growth factor, and 0.1% gentamicin and amphotericin-B (GA-1000), all purchased from Lonza. At 70% to 90% confluence, BAEC were sub-cultured with HEPES buffered saline solution (Lonza) followed by 0.25 mg/ml trypsin/EDTA solution (Lonza) to detach cells from their substrate. The cells were transferred to fibronectin-coated glass slides (30 µg/mL, Corning), seeded at a cell density of 5,000 cells/cm², and allowed to grow to confluency for 3-5 days.

Glycocalyx Stabilization: For two hours prior to and during the shear stress experiments, BAEC were cultured in fully supplemented growth medium containing a reduced concentration of FBS (2.5%) along with bovine serum albumin (BSA; 0.5%) to stabilize the GCX. This medium is referred to as experimental medium.

HS Degradation: For short term shear stress experiments, HS was enzymatically degraded by adding *F. heparinum* heparinase III (HepIII) to the experimental medium during the two hour pre-flow period. For 24-hour shear stress experiments, HS was enzymatically degraded by HepIII treatment during the initial two hour pre-flow period and also throughout the duration of the flow experiment. The purpose of maintaining the presence of HepIII enzyme for the 24-hour flow experiment was to prevent the potential onset of HS restoration that occurs hours to days after enzyme removal⁵³. As previously described, HepIII was used at a concentration of 15 mU/mL when obtained from Sigma. Occasionally, HepIII was obtained from IBEX Technologies Inc. and the concentration used was also 15 mU/mL, determined by converting IBEX international units (I.U.) to Sigma units (1 I.U. is equivalent to 600 Sigma units). HS degradation was confirmed by immunofluorescence microscopy of aldehyde-fixed BAEC stained with anti-mouse heparan sulfate (HepSS-1) monoclonal antibody (US Biological). HS fluorescent images of untreated and HepIII-treated monolayers were recorded at using uniform camera

settings. NIH ImageJ was employed to analyze the images, subtract background fluorescence, and measure fluorescence intensity by calculating the illuminated fraction (percent) of the total field of view.

GPC1 and SDC1 Silencing: GPC1 and SDC1 were gene silenced via RNA interference (RNAi). Specifically, EC monolayers were plated in 35-mm diameter culture treated petri dishes in GA-1000-free culture medium. At 60% confluence, the EC were transfected with 4 µg of bovine-specific GPC1 or SDC1 short hairpin RNA (shRNA) obtained from Santa Cruz Biotechnology. The bovine GPC1 and SDC1 shRNA plasmids were each a pool of 3 shRNA plasmids which are listed in the table 1.

Glypican-1 shRNA	
Plasmid A	5'-GATCCCGCCTATAATGGCAACGATTTCAAGAGAATCGTTGCCATTATAGGCGTTTTT-3' corresponds to siRNA sense 5'-CGCCUAUAAUGGCAACGAUtt-3' and anti-sense 5'-AUCGUUGCCAUAUAGGCGtt-3'
Plasmid B	5'-GATCCCAGCAGACGATATTTAACTTTCAAGAGAAGTTAAATATCGTCTGCTGTTTTT-3' corresponds to siRNA sense 5'-CAGCAGACGAUUAUUUAACUtt-3' and anti-sense 5'-AGUUAAAUAUCGUCUGCUGtt-3'
Plasmid C	5'-GATCCCTTCGAGTCCTCGTATGAATTCAGAGATTCATACGAGGACTCGAAGTTTTT-3' corresponds to siRNA sense 5'-CUUCGAGUCCUCGUUAUGAAtt-3' and antisense 5'-UUCAUACGAGGACUCGAAGtt-3'
Syndecan-1 shRNA	
Plasmid A	5'-GATCCGGTCTAACTTAGATGTCAATTCAGAGATTGACATCTAAGTTAGACCTTTTTT-3' corresponds to siRNA sense 5'-GGUCUAACUUAGAUGUCAAtt-3' and antisense 5'-UUGACAUCUAAGUUAGACtt-3'
Plasmid B	5'-GATCCCCAATGTCTAGGTTAGTTTTCAAGAGAAAACCTAGACATTGGTTTTT-3' corresponds to siRNA sense 5'-CCAAUGUCUAGGUUAGUUUtt-3' and antisense 5'-AAACUAACCUAGACAUUGGtt-3'
Plasmid C	5'-GATCCGTAGTCATGTGAACCTAATTCAGAGATTAGAGTTCACATGACTACTTTTTT-3' corresponds to siRNA sense 5'-GUAGUCAUGUGAACUCUAAAtt-3' and antisense 5'-UUAGAGUUCACAUGACUACTt-3'

Table 1: Glypican-1 and syndecan-1 shRNA sequences are specified.

12 µl of Optifect transfection reagent (Invitrogen) in 2 ml of reduced-serum OptiMEM (Invitrogen) transfection medium was used to facilitate the transfection. For control purposes, groups of EC monolayers were (i) not transfected, (ii) transfected with OptiMEM, Optifect, the vector (in which the shRNA was packaged to facilitate introduction of the shRNA in the cells), and scrambled shRNA sequences (proprietary; Santa Cruz Biotechnology), or (iii) transfected with OptiMEM, Optifect, the empty vector, and GFP. After 12 hours, the transfection medium was replaced with GA-1000-free culture medium. After another 36 hours, to generate stably transfected cell lines, 2.5 µg/ml of puromycin antibiotic was added to the culture medium along with the original 0.1% GA-1000. GPC1

and SDC1 protein suppression were demonstrated by Western blots and densitometric analyses (see further methods below). The transfection was allowed to stabilize, and cells were expanded, usually within two weeks before shear stress experiments were performed. During shear stress experiments, GPC1 and SDC1 knockdown BAEC were exposed to puromycin-containing experimental medium.

Shear Stress Experiments: BAEC were sheared in a parallel plate flow chamber (C&L Instruments) for 3 or 6 hours, or BAEC were sheared in a rotating disk flow apparatus (supplemental information) for 24 hours. In the parallel plate flow chamber, with a cell contact surface area of 6.6 cm^2 and a channel height of $250 \text{ }\mu\text{m}$, confluent BAEC monolayers were sheared at 15 dyne/cm^2 . Since all cells were exposed to the same magnitude of shear stress, the entire monolayer was suitable for protein quantification. Fluid was driven through the parallel plate chamber from a multi-head peristaltic pump (Rainin) then via a vibration damper, followed by the flow chamber, and finally a receiving reservoir before being re-circulated. The rotating disk apparatus was custom designed to shear BAEC grown in a 6-well plate, in order to maximize the number of experiments that could be performed in a 24-hour time period (supplemental information). In each well, the cell contact surface was 2.7 cm^2 on a 3.1-cm diameter round glass coverslip fixed to the bottom of the well using sterile silicone grease (supplemental information). 6 cylindrical disks were suspended at $500 \text{ }\mu\text{m}$ above 6 cell layers. Using a motor drive, the disks were simultaneously rotated at the number of rotations per minute required to generate an average shear stress of 14 dyne/cm^2 (supplemental information). The parallel plate and rotating disk flow systems were both maintained in an incubator at $37 \text{ }^\circ\text{C}$ with a supply of $5\% \text{ CO}_2$. At the end of the experiments, samples were processed as described below.

Whole Cell Protein Extraction and Western Blotting: Whole cell protein was extracted from cells using lysis buffer containing 1 mM sodium bicarbonate, 2 mM phenylmethylsulphonyl fluoride, 1 mM sodium orthovanadate, 5 mM EDTA, and 1X complete protease inhibitor cocktail (Roche Laboratories). After scraping and collecting the cells, the extracts were sonicated briefly and frozen at -80°C overnight. Equal protein amounts ($10 \text{ }\mu\text{g/lane}$) were determined by the BCA protein assay kit (Pierce) and resolved on 7.5% sodium dodecyl sulfate polyacrylamide gel electrophoresis (SDS-PAGE)

gels. Protein was transferred to nitrocellulose membranes (Whatman), which were blocked by incubation for 30 minutes at room temperature with TBS containing 0.5% Tween-20 (TBS-T) and 5% nonfat dry milk. Membranes were then incubated overnight at 4°C with primary antibody. Primary antibodies were against Ser¹¹⁷⁷ phosphorylated eNOS (1:1000) and total eNOS (1:2500) (both from Cell Signaling), glypican-1 (1:10000; characterized and provided by Dr. Richard Margolis, NYU Langone Medical Center⁵⁴), syndecan-1 (1:1000; clone H-174 from Santa Cruz Biotechnology), and β -actin (1:10000; Sigma). On the following day, membranes were incubated for 2 hours at room temperature with secondary label. Secondary labeling was accomplished with horseradish peroxidase-conjugated goat anti-rabbit IgG (1:10000; Santa Cruz Biotechnology) for all proteins of interest, except β -actin which was secondarily labeled with horseradish peroxidase-conjugated goat anti-mouse IgG (1:10000; Santa Cruz Biotechnology). After incubation of membranes with Immobilon Western Detection Reagents (Millipore), detection of protein bands was performed using a Carestream Image Station 4000MM Pro and Carestream Molecular Imaging (MI) software. Densitometry measurements were achieved using ImageJ.

Assessment of Cell Remodeling: To evaluate cell morphology and orientation angle, BAEC were imaged by phase contrast microscopy. ImageJ was used to trace the perimeters of individual BAEC and determine their aspect ratios (AR), defined as $AR = (\text{long axis})/(\text{short axis})$. The aspect ratio was near 1 for a round or cobblestone-shaped EC and much higher than 1 for elongated cells. We also used ImageJ to calculate the angles of the BAEC long axes relative to the direction of flow. Relative angles were grouped and plotted in 20° intervals. For each condition of interest we performed 4 independent experiments. Per experiment, we examined 3 randomly distributed fields in each of two BAEC monolayers. We quantified the aspect ratios of 30 cells per field, but only when BAEC monolayers were intact.

For short term flow exposure studies in which changes in cell shape and flow-directed alignment that are less striking, cytoskeleton reorganization was also evaluated to assess cell remodeling. This was achieved by examining f-actin redistribution. BAEC were fixed in 4% paraformaldehyde for 10

minutes, permeabilized in 0.2% triton X-100, and blocked in 3% goat serum/0.2% triton X-100. Cell monolayers were then treated with Alexa Fluor 594 conjugated F-actin Phalloidin (Molecular Probes) diluted in 3% BSA. 4',6-diamidino-2-phenylindole (DAPI) marked the EC nuclei. BAEC cytoskeleton and nucleus fluorescence were visualized with a Zeiss LSM 510 confocal laser scanning system and Zeiss LSM software, a 60X/Oil objective, and by z-stacking.

Statistical Analysis: HS fluorescence intensity data sets were averaged and normalized by untreated control values. Results are expressed as mean \pm SEM. The data set was analyzed using the unpaired two-tailed t-test to determine the statistical significance of mean differences. SDC1 and GPC1 protein levels were averaged, normalized by baseline values, expressed as mean \pm SEM, and statistically analyzed using ANOVA and the Student-Newman-Keuls (SNK) test. P-eNOS, total eNOS, and beta-actin protein levels were statistically analyzed in the same way. Fold changes in aspect ratio and angles of orientation were averaged and expressed as mean \pm SEM. The statistical and mean comparisons tests used to analyze the aspect ratio data were ANOVA and SNK. To analyze alignment we used the t-test and Sidak-Bonferroni method to compare means within each range of angle orientation. F-actin fiber orientation within cell bodies was qualitatively analyzed.

CONCLUSION

Our findings provide evidence that HS is involved in both centralized and decentralized GCX-mediated mechanotransduction mechanisms. GPC1 plays a role as a centralized mechanotransmitter in the eNOS-containing caveolar compartment of the plasma membrane. SDC1 functions in decentralizing mechanotransmitter via the cytoskeleton. This foundational work in EC may translate to other flow sensing cells (e.g., vascular smooth muscle cells and cancer cells) and to the development of methods to stabilize or rebuild the GCX and its core proteins in order to ensure proper EC function as a treatment for vascular disease.

ACKNOWLEDGEMENTS

We acknowledge the support of the National Institutes of Health, through the following grants: 5T32HL007675, HL57093, and HL094889. We also appreciate the contributions of: Dr. Richard Margolis (New York University Langone Medical Center) for donating glypican-1 antibody; Dr. Xingying Ji (City College of New York) and Ms. Marcia Urban-Maldonado (Albert Einstein College of Medicine) for shRNA transfection technical support.

REFERENCES

1. M. P. McKinley and V. D. O'Loughlin, *Human anatomy*, 3rd edn., McGraw-Hill, New York, 2012.
2. J. A. Florian, J. R. Kosky, K. Ainslie, Z. Pang, R. O. Dull and J. M. Tarbell, *Circ Res*, 2003, **93**, e136-142.
3. M. Y. Pahakis, J. R. Kosky, R. O. Dull and J. M. Tarbell, *Biochem Biophys Res Commun*, 2007, **355**, 228-233.
4. M. M. Thi, J. M. Tarbell, S. Weinbaum and D. C. Spray, *Proc Natl Acad Sci U S A*, 2004, **101**, 16483-16488.
5. Y. Yao, A. Rabodzey and C. F. Dewey, Jr., *Am J Physiol Heart Circ Physiol*, 2007, **293**, H1023-1030.
6. J. C. Lewis, R. G. Taylor, N. D. Jones, R. W. St Clair and J. F. Cornhill, *Lab Invest*, 1982, **46**, 123-138.
7. B. M. van den Berg, J. A. Spaan, T. M. Rolf and H. Vink, *Am J Physiol Heart Circ Physiol*, 2006, **290**, H915-920.
8. H. C. Stary, A. B. Chandler, R. E. Dinsmore, V. Fuster, S. Glagov, W. Insull, Jr., M. E. Rosenfeld, C. J. Schwartz, W. D. Wagner and R. W. Wissler, *Circulation*, 1995, **92**, 1355-1374.
9. T. J. Tegos, E. Kalodiki, M. M. Sabetai and A. N. Nicolaidis, *Angiology*, 2001, **52**, 89-98.
10. Z. D. Shi and J. M. Tarbell, *Ann Biomed Eng*, **39**, 1608-1619.
11. Z. D. Shi, H. Wang and J. M. Tarbell, *PLoS One*, **6**, e15956.
12. Z. D. Shi, G. Abraham and J. M. Tarbell, *PLoS One*, **5**, e12196.
13. Z. D. Shi, X. Y. Ji, D. E. Berardi, H. Qazi and J. M. Tarbell, *Am J Physiol Heart Circ Physiol*, **298**, H127-135.
14. Z. D. Shi, X. Y. Ji, H. Qazi and J. M. Tarbell, *Am J Physiol Heart Circ Physiol*, 2009, **297**, H1225-1234.
15. H. Qazi, Z. D. Shi and J. M. Tarbell, *PLoS One*, **6**, e20348.
16. O. Traub and B. C. Berk, *Arterioscler Thromb Vasc Biol*, 1998, **18**, 677-685.

17. J. J. Chiu and S. Chien, *Physiol Rev*, **91**, 327-387.
18. P. F. Davies, *Physiol Rev*, 1995, **75**, 519-560.
19. J. M. Tarbell and M. Y. Pahakis, *J Intern Med*, 2006, **259**, 339-350.
20. A. Oohira, T. N. Wight and P. Bornstein, *J Biol Chem*, 1983, **258**, 2014-2021.
21. Y. Zeng, M. Waters, A. Andrews, P. Honarmandi, E. Ebong, V. Rizzo and J. M. Tarbell, *Am J Physiol Heart Circ Physiol*.
22. R. D. Rosenberg, N. W. Shworak, J. Liu, J. J. Schwartz and L. Zhang, *J Clin Invest*, 1997, **99**, 2062-2070.
23. Y. Halden, A. Rek, W. Atzenhofer, L. Szilak, A. Wabnig and A. J. Kungl, *Biochem J*, 2004, **377**, 533-538.
24. R. Kokenyesi and M. Bernfield, *J Biol Chem*, 1994, **269**, 12304-12309.
25. M. D. Bass and M. J. Humphries, *Biochem J*, 2002, **368**, 1-15.
26. M. Simons and A. Horowitz, *Cell Signal*, 2001, **13**, 855-862.
27. L. A. Fransson, M. Belting, F. Cheng, M. Jonsson, K. Mani and S. Sandgren, *Cell Mol Life Sci*, 2004, **61**, 1016-1024.
28. M. Belting, K. Mani, M. Jonsson, F. Cheng, S. Sandgren, S. Jonsson, K. Ding, J. G. Delcros and L. A. Fransson, *J Biol Chem*, 2003, **278**, 47181-47189.
29. F. Cheng, K. Mani, J. van den Born, K. Ding, M. Belting and L. A. Fransson, *J Biol Chem*, 2002, **277**, 44431-44439.
30. R. G. Parton and K. Simons, *Nat Rev Mol Cell Biol*, 2007, **8**, 185-194.
31. T. Arisaka, M. Mitsumata, M. Kawasumi, T. Tohjima, S. Hirose and Y. Yoshida, *Ann N Y Acad Sci*, 1995, **748**, 543-554.
32. W. Duan, L. Paka and S. Pillarisetti, *Cardiovasc Diabetol*, 2005, **4**, 16.
33. L. Paka, Y. Kako, J. C. Obunike and S. Pillarisetti, *J Biol Chem*, 1999, **274**, 4816-4823.
34. J. Turnbull, A. Powell and S. Guimond, *Trends Cell Biol*, 2001, **11**, 75-82.
35. P. Vijayagopal, J. E. Figueroa and E. A. Levine, *J Surg Oncol*, 1998, **68**, 250-254.

36. M. Yanagishita and V. C. Hascall, *J Biol Chem*, 1992, **267**, 9451-9454.
37. S. V. Lopez-Quintero, R. Amaya, M. Pahakis and J. M. Tarbell, *Am J Physiol Heart Circ Physiol*, 2009, **296**, H1451-1456.
38. E. Tkachenko, J. M. Rhodes and M. Simons, *Circ Res*, 2005, **96**, 488-500.
39. G. Garcia-Cardena, P. Oh, J. Liu, J. E. Schnitzer and W. C. Sessa, *Proc Natl Acad Sci U S A*, 1996, **93**, 6448-6453.
40. E. E. Ebong, F. P. Macaluso, D. C. Spray and J. M. Tarbell, *Arterioscler Thromb Vasc Biol*, **31**, 1908-1915.
41. R. O. Dull, M. Cluff, J. Kingston, D. Hill, H. Chen, S. Hoehne, D. T. Malleske and R. Kaur, *Am J Physiol Lung Cell Mol Physiol*, **302**, L816-828.
42. M. Nikmanesh, Z. D. Shi and J. M. Tarbell, *Biotechnol Bioeng*, **109**, 583-594.
43. R. O. Dull, I. Mecham and S. McJames, *Am J Physiol Lung Cell Mol Physiol*, 2007, **292**, L1452-1458.
44. J. J. Moon, M. Matsumoto, S. Patel, L. Lee, J. L. Guan and S. Li, *J Cell Physiol*, 2005, **203**, 166-176.
45. R. Kumagai, X. Lu and G. S. Kassab, *Free Radic Biol Med*, 2009, **47**, 600-607.
46. J. W. VanTeeffelen, J. Brands, C. Jansen, J. A. Spaan and H. Vink, *Hypertension*, 2007, **50**, 261-267.
47. K. M. Ainslie, J. S. Garanich, R. O. Dull and J. M. Tarbell, *J Appl Physiol*, 2005, **98**, 242-249.
48. R. T. Megens, S. Reitsma, P. H. Schiffers, R. H. Hilgers, J. G. De Mey, D. W. Slaaf, M. G. oude Egbrink and M. A. van Zandvoort, *J Vasc Res*, 2007, **44**, 87-98.
49. J. Robinson and D. Gospodarowicz, *J Cell Physiol*, 1983, **117**, 368-376.
50. J. M. Tarbell and E. E. Ebong, *Sci Signal*, 2008, **1**, pt8.
51. D. M. Beauvais, B. J. Burbach and A. C. Rapraeger, *J Cell Biol*, 2004, **167**, 171-181.
52. K. J. McQuade, D. M. Beauvais, B. J. Burbach and A. C. Rapraeger, *J Cell Sci*, 2006, **119**, 2445-2456.

53. A. Koo, C. F. Dewey, Jr. and G. Garcia-Cardena, *Am J Physiol Cell Physiol*, **304**, C137-146.
54. L. Karthikeyan, M. Flad, M. Engel, B. Meyer-Puttlitz, R. U. Margolis and R. K. Margolis, *J Cell Sci*, 1994, **107 (Pt 11)**, 3213-3222.

FIGURE LEGENDS

Figure 1: EC monolayer heparan sulfate fluorescence intensity. (A) Enface perspective of an untreated HS-stained BAEC monolayer viewed using an inverted fluorescence microscope; Bar = 100 μ m. (B) Enface inverted fluorescence microscope perspective of HepIII-treated and HS-stained BAEC monolayer; Bar = 100 μ m. (C) Quantification (normalized) of control (untreated) and HepIII-treated BAEC monolayer fluorescence intensity of HS. *P < 0.05; n=3.

Figure 2: ShRNA transfection. (A) GFP-expressing control shRNA demonstrates shRNA stable transfection efficiency; Bar = 25 μ m. (B) Western blots were performed for control, GPC1, and SDC1 shRNA transfections. We assessed whole cell protein levels of GPC1 and SDC1. β -actin was probed as a loading control. In the left panel of Western blots lane 1 is an untreated control, lane 2 is a scrambled shRNA control, and lane 3 is the GFP-expressing shRNA control; all bands are similar for all conditions, as expected. In the middle panel of Western blots lane 4 is an untreated control and lane 5 is the GPC1 shRNA treatment; the change in GPC1 is expected and it is accompanied by a change in SDC1. In the right panel of Western blots lane 6 is an untreated control and lane 7 is the SDC1 shRNA treatment; the change in SDC1 is expected and there is no change in GPC1. (C, D) Plots are based on GPC1 shRNA and SDC1 shRNA knockdown of whole cell GPC1 and SDC1 protein as determined using Western blots and densitometric analysis. **P \leq 0.01 or ***P \leq 0.001; n = 6.

Figure 3: Western blots were performed to probe ser1177 phosphorylated eNOS (p-eNOS), total eNOS, and β -actin (loading control). This figure shows: (A and B) HS related Western blots and densitometry; (C and D) GPC1 related Western blots and densitometry; and (E and F) SDC1 related Western blots and densitometry. Lanes 1, 5, 9 are control BAEC; lane 2 is control and HepIII-treated BAEC; lane 6 is control and GPC1 shRNA-treated BAEC; lane 10 is control and SDC1 shRNA-treated BAEC; lanes 3, 7, 11 are sheared BAEC; lane 4 is sheared and HepIII-treated BAEC; lane 8 is shear

and GPC1 shRNA-treated BAEC; and lane 12 is shear and SDC1 shRNA-treated BAEC. Numbers 1 through 12 follow the order of the bar plots, which quantify the p-eNOS densitometric analysis. P-eNOS densitometry values were normalized by beta-actin, followed by total eNOS, and finally by the control. The data was averaged and is expressed as mean +/- SEM. *P < 0.05 is statistically significant compared to other conditions in the data set; #P < 0.05 is statistically significant compared to control (unsheared) SDC1 shRNA; n = 8 EC monolayers per condition studied.

Figure 4: HS, not GPC1, regulates BAEC morphology. (A-D) This figure shows phase contrast images of untreated cells exposed to no shear, 24-hour sheared cells that were not treated, 24-hour sheared cells that were HepIII-treated, and 24-hour sheared cells that were GPC1 shRNA-treated, respectively. The direction of flow is indicated by the arrow; bar = 50 μ m. (E-H) Quantification of cell elongation and alignment with flow direction; grey bars represent data from no shear conditions and black bars represent data from sheared conditions. (E) BAEC elongation was quantified by measuring the aspect ratios (AR = long axis / short axis), which approach 1 when cells are cobblestone-shaped and are greater than 1 when cells are elongated. Control EC aspect ratios were variable, depending on the EC batch. Therefore, fold changes in aspect ratio are presented in place of raw values. The normalized aspect ratio of the control EC shown in figure 4A has a value of 1. We quantified fold changes in aspect ratio due to other conditions by dividing by raw control values. (F) Percent of untreated cells, (G) percent of HepIII-treated cells, and (H) percent of GPC1 shRNA-treated cells oriented 0 to \pm 90° relative to the direction of flow are also presented in this figure. *P \leq 0.05, ***P \leq 0.001, † P \leq 0.05 (elongation with GPC1 shRNA treatment compared to elongation with no treatment), or †††P \leq 0.001 (elongation with HepIII treatment compared to elongation with no treatment or GPC1 shRNA treatment); Alignment with no treatment was not found to be statistically different than alignment with GPC1 shRNA treatment, with a P value of 0.0139535; 30 cells in each of 18 to 24 monolayer fields were studied per condition and, thus, n = 540 to 720.

Figure 5: SDC1 regulates flow-induced BAEC cytoskeleton reorganization. Phase contrast images and F-actin fluorescence images are shown, of (A) untreated cells exposed to no shear, (B) 6-hour sheared cells that were not treated, and (C) 6-hour sheared cells that were SDC1 shRNA-treated. The direction of flow is indicated by the arrow. Phase contrast image bar = 50 μm . Fluorescent image bar = 10 μm . (D) BAEC elongation is quantified by measuring aspect ratios and computing fold changes in aspect ratio compared to control conditions. (E, F) Quantification of cell alignment indicates the percentage of cells oriented an average of -80 to +80 degrees relative to the direction of flow. (E) Untreated BAEC. (F) SDC1 shRNA-treated BAEC. Grey bars represent data from no shear conditions and black bars represent data from sheared conditions. * $P \leq 0.05$ or *** $P \leq 0.001$; 30 cells in each of 18 to 24 monolayer fields were studied per condition and, $n = 540$ to 720.

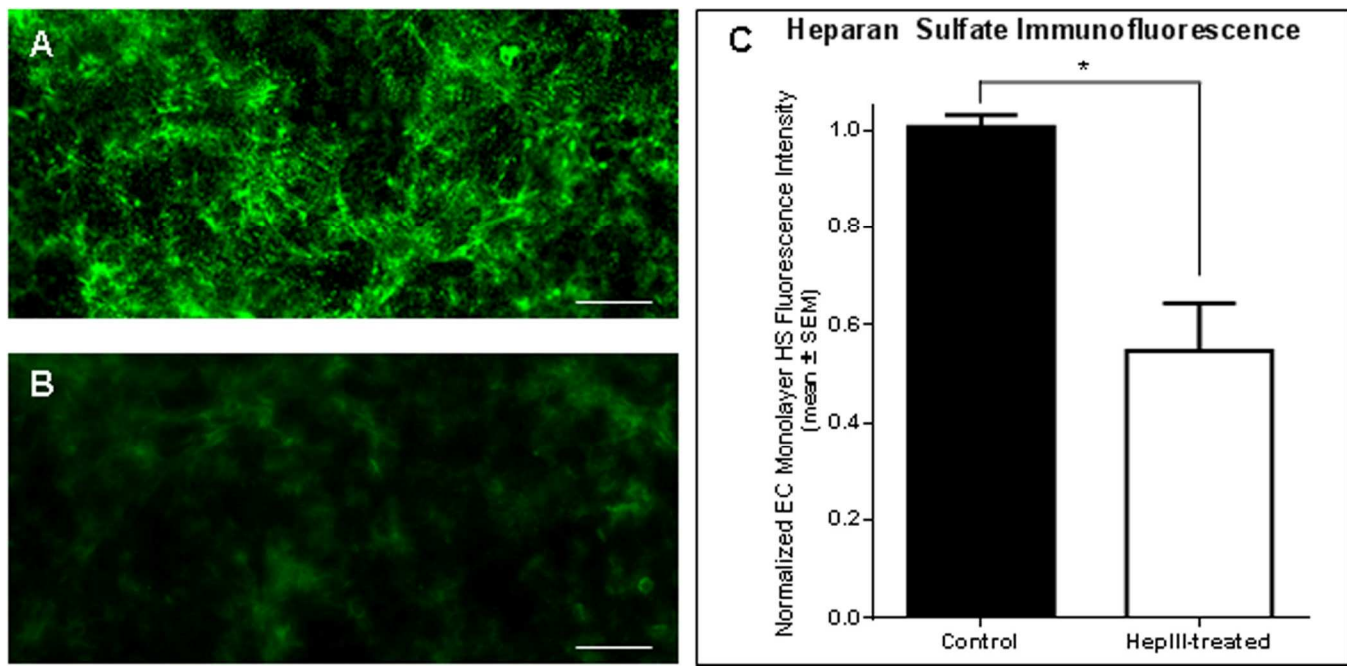


Figure 1

Integrative Biology Accepted Manuscript

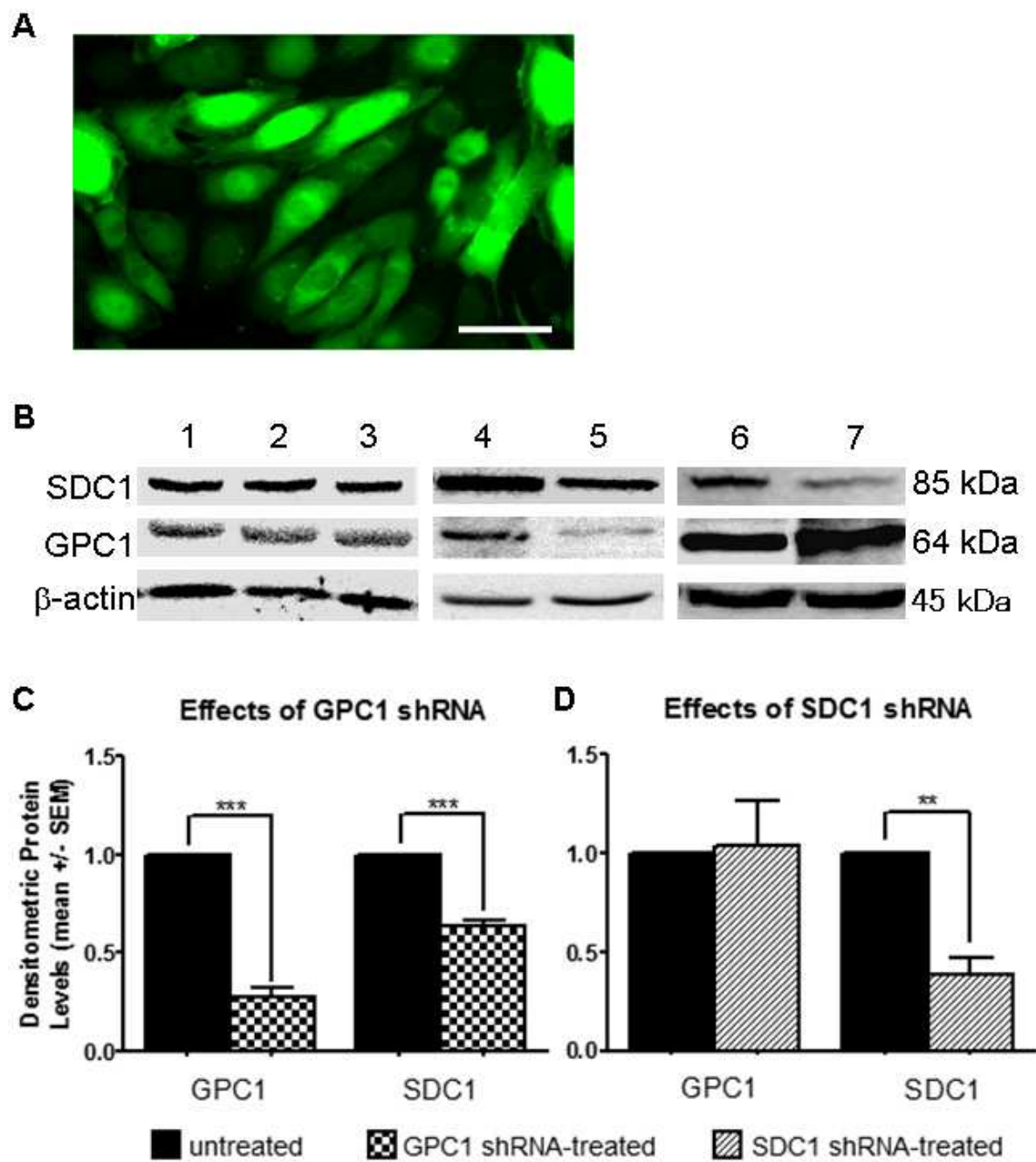


Figure 2

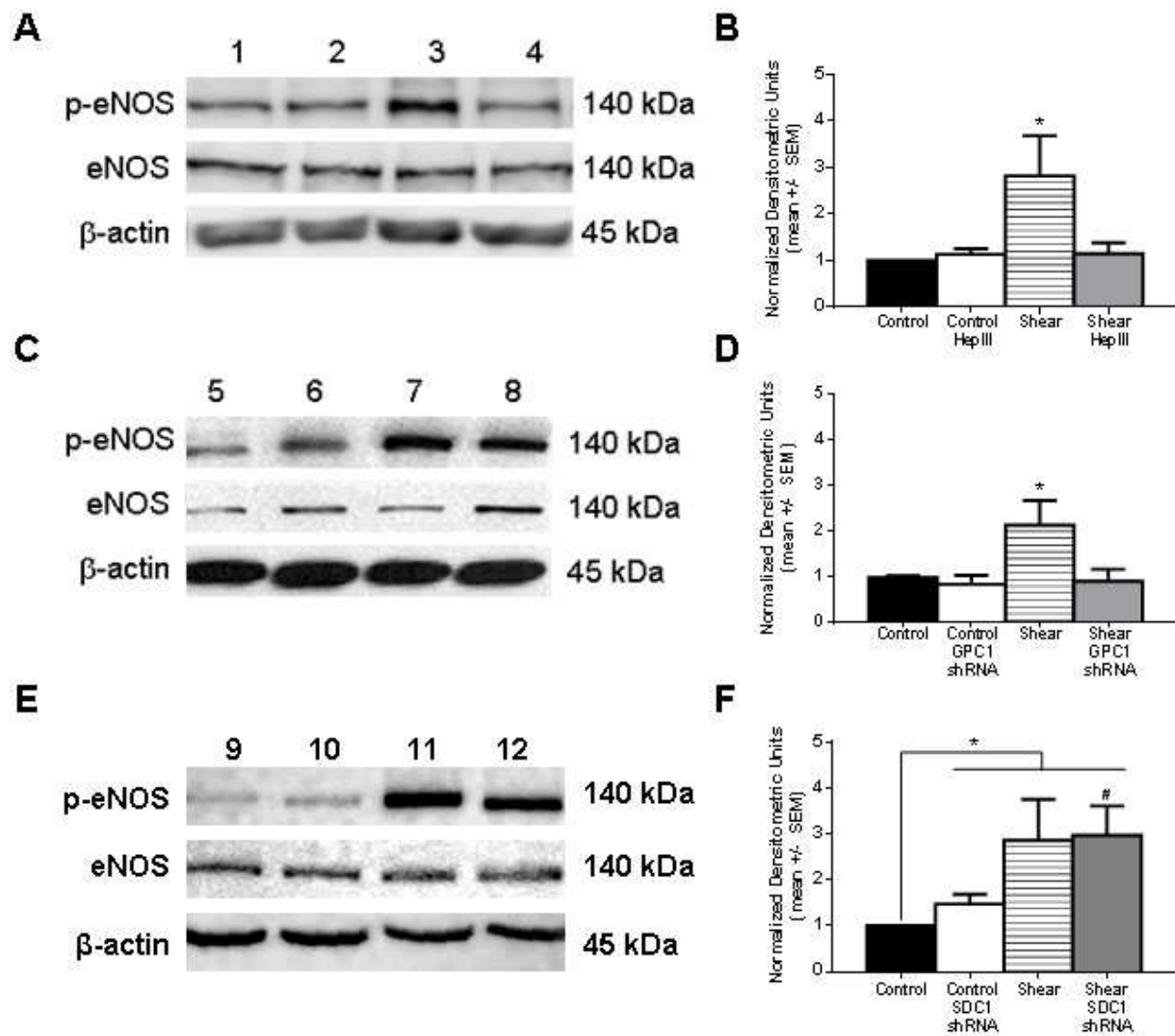


Figure 3

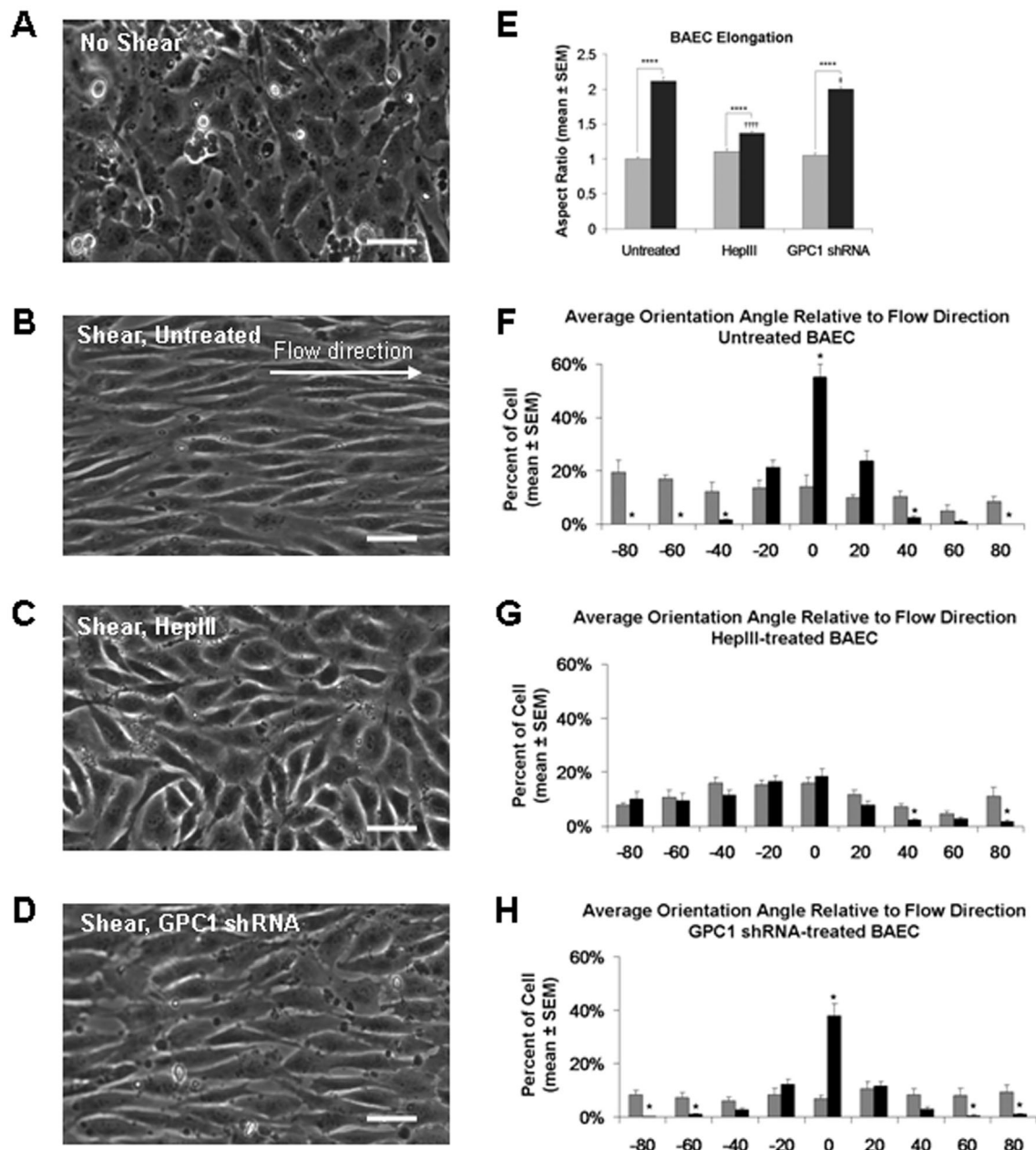


Figure 4

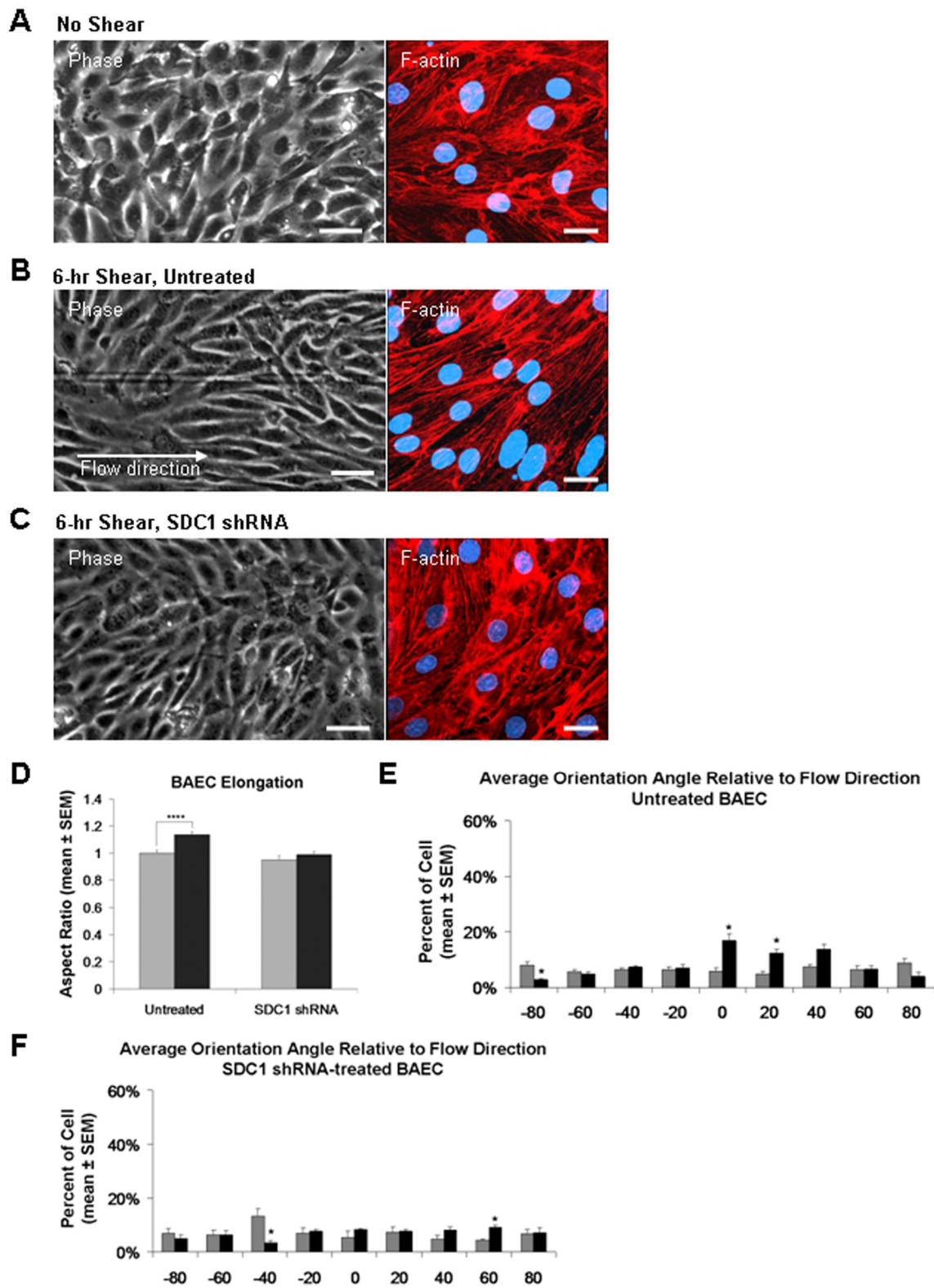


Figure 5